Supporting information

Chow et al. 10.1073/pnas.1217691110

SI Text

Note 1. The central role of the posterior cingulate cortex (PCC) proposed by Vogt and Laureys (1) is consistent with work demonstrating that PCC activity is positively correlated with activity in the thalamus, and that both vary directly with the level of consciousness (2) during waking and in various states of clinical impairment. Importantly, these relationships have not until now been examined during rapid eye movement (REM) sleep.

Note 2. A recent study (3) explored the strength of connectivity among default mode network (DMN) core regions throughout the sleep-wake cycle, and reported that this remained consistent across all sleep-wake stages, contrary to a number of other studies (4–7). These discrepancies may be because of methodological differences; for example, there were no apparent measurements of, or correction for the effect of physiological variables, such as respiration and heart rate, which might have had an impact on the magnitude of estimated correlation coefficients.

Note 3. It should be noted that there have been previous reports of experimental circumstances [e.g., mind wandering in humans (8, 9) or anesthesia in nonhuman primates (10)] in which the expected anticorrelations between the DMN and these attentional networks appear to break down.

Note 4. Anatomical tract tracing studies (11–13) suggest that the reciprocal relationship between the DMN and unimodal cortices cannot be mediated wholly by direct intracortical pathways because medial prefrontal and PCC/retrosplenial (RSP) cortices do not project directly to many of the unimodal areas. However, both the medial prefrontal cortex (MPFC) and PCC/RSP project to the pulvinar (13, 14), which is the thalamic region with which they are most strongly coupled during REM. The pulvinar, in turn, has reciprocal projections to the unimodal visual, auditory, and somatosensory areas (15, 16), placing it in a position to orchestrate the large-scale dissociations that we observe during REM. The pulvinar receives the vast majority of its primary "driver" afferents from the cortex itself rather than from ascending pathways. These type II corticothalamic fibers appear to serve as a feed-forward mechanism that, via second order projections back to the cortex, transmit information from one cortical area to another, the means by which the pulvinar, as a thalamic association nucleus, is able to modulate cortico-cortical communication (17).

Note 5. Viewed from the perspective of the thalamus, the patterns described might also represent the interplay between two attentional systems that have become functionally segregated during REM: (*i*) a bottom up network, in which the pulvinar may again play a central role [see Grieve et al. (18)], that orients attention toward, and organizes rapid motor responses to sensory, particularly complex visual, stimuli (18); and (*ii*) a supervisory attentional system instantiated in a set of a heteromodal regions that exerts top down executive control over these processes (19, 20).

Note 6. A suggestion of these relationships can be found in the results of prior imaging studies (21–25). However, the static contrast methods used in those studies have given the consistent impression that unimodal sensorimotor activity, when present, was predominant. These methods did not support detection of the reciprocal fluctuating pattern we report here.

Note 7. Previous human neuroimaging studies have revealed associations between REM bursts and activity in sensorimotor areas (26–28) that may correspond to the intermittent activation of these regions we report here [but see also Hong et al. (22)]. These studies used event-related contrast methods or acquired data during the presentation of auditory stimuli, whereas the resting-state connectivity methods used in the present study afford a different perspective: baseline-free, stimulus-independent, and capable of tracking the continuous flow of information over time. It is interesting to note that studies using methods in which the temporal resolution is superior to both blood-oxygen level-dependent (BOLD) contrast or PET methods, report findings that are consistent with the intermittent activation of heteromodal regions we observe during REM; for example, Kubota et al. (29), using infrared spectroscopy, reported transient fluctuation in oxygenation of the prefrontal cortex during REM sleep.

Note 8. Infraslow oscillations of the EEG [below 0.1 Hz, an order-of-magnitude slower than the ∼1 Hz slow waves that characterize slow-wave sleep (SWS)], likely regulated by the thalamus, have been described for many years (30–32), as have rhythmic fluctuations in the BOLD signal below 0.1 Hz (33). [Indeed one of the principal ways the DMN (34) and other resting-state networks (35) are defined is in terms of coherence of functional MRI (fMRI) fluctuations at these frequencies (36)]. Indeed, it has been proposed that slow cortical oscillations themselves may be an important contributor to the BOLD signal (37). Infraslow fluctuations in both BOLD and EEG signals have been described during sleep (32, 38, 39). Furthermore, although the precise relationship between them is unclear, recent reports suggest a correspondence between infraslow oscillations of the EEG and infraslow variations in the BOLD signal during sleep (although stage-specific differences were not evaluated) (40).

Note 9. Phasic phenomena observed during REM occurring at roughly the same time scale—between 0.1 and 0.01 Hz—include REM-specific spike densities in mesencephalic locomotor nuclei and ventrolateral medulla (peaking at roughly 20- to 60-s intervals) (41, 42) and sawtooth wave periodicities (43, 44). In addition, ponto-geniculo-occipital wave activity may show bursting properties at similarly slow intervals (45, 46), which is also the frequency of the "cyclic alternating pattern" that has been described during sleep (47).

Note 10. Converging evidence suggests that slow oscillations (less than 1 Hz) facilitate synchronization of neural activity between brain regions (48). These oscillations reflect alternation of membrane potentials between hyperpolarized (down state) and relatively depolarized (up state) conditions that have been used to interpret cortical patterns seen during non-REM sleep (49). During REM, perhaps modulated by thalamic or neurochemical mechanisms, these oscillations might become synchronized but out of phase, in sensorimotor and heteromodal systems. The sequential alternation of up and down states in these systems might represent a mechanism for the reciprocal activations in time that we observe.

Note 11. Although there is evidence supporting the idea from animal (50, 51) and human studies (52–54)—and although it is consistent with the notion that sleep-related slow oscillations facilitate synaptic strength via cortico-cortical interactions (55)—REM-facilitated consolidation of procedural memory (or any kind of memory) in humans remains controversial (56).

SI Methods

MRI Data Acquisition. fMRI data were acquired on a 3T scanner (GE Signa) with a 16-channel receive-only detector array. Foam pads were used to restrict subject's head motion. For the comfort of the subjects, a foam mattress pad was placed on the scanner table. BOLD fMRI was acquired using an echo planar imaging (EPI) sequence. Primary data collection was preceded by a short functional run that included 10 different echo times (TE), to be used as a reference for correction of geometric distortions (2). Each EPI volume included 25 axial slices, which covered most of the brain (3.45×3.45 mm^2 in-plane resolution, 4.5-mm thickness, 0.5-mm gap). Other scanning parameters were as follows: repetition time (TR) = 3 s, TE = 45 ms, flip angle = 90°, and a maximum of 3,600 image repetitions. To facilitate sleep, the acoustic noise generated by the EPI sequence was kept below a sound pressure level of 96 dBA by decreasing the bandwidth to 62.54 kHz and limiting the gradient slew-rate to 25 T·m·s. Subjects also wore earplugs for further sound attenuation. For the functional data acquired during resting wakefulness, the same parameters were used.

In addition to the fMRI data, T2-weighted anatomical images (fast spin echo, FSE) were collected at the same slices as the functional data and used for distortion correction and coregistration. T1-weighted (magnetization-prepared rapid acquisition gradient echo, MPRAGE) anatomical images were collected in a separate scan session using the product birdcage head-coil.

A pneumatic squeeze-ball, which was connected to set off a sound alarm, was provided to the volunteers. The subjects were instructed to squeeze the ball at any point if they felt uncomfortable, wanted to interrupt the study, or wanted to communicate with the researchers. If the session was interrupted and the subject agreed to continue, additional T2-weighted anatomical images were acquired to allow for correction for potential altered changes in head position.

EEG and Physiologic Recordings. Electrical scalp recordings were made using sintered silver–silver chloride electrode caps with BrainAmp-MRplus amplifiers, and Acquire software (Brain Products). Electrodes were placed in a subset of locations of the 10–20 International System. The reference electrode was located between Fz and Cz and the ground electrode below Oz, all on the brain midline. An electrode was placed below the right eye to monitor the electrooculogram and another on the subject's back, to monitor the cardiac signal. A bipolar set of electrodes was placed on the chin to monitor submentalis muscular tone. These electrodes were connected to a bipolar amplifier (BrainAmp-ExG-MR; Brain Products) connected to the same acquisition system as the EEG channels. The data acquisition rate was 5 kHz, with an analog band-pass filter set to 0.016–250 Hz. Data were collected in a continuous fashion. Respiration was measured using a respiratory bellows placed on the chest, and cardiac rate was measured using a pulse oximeter placed on the left index finger. Both transducers are standard equipment on the GE Signa MRI scanner. Signals from the respiratory and cardiac sensors and MRI scanner-generated trigger pulses were collected, using in-house software, at a frequency of 1 kHz.

EEG Data Analysis. Artifacts related to gradient switching and cardioballistic effects were removed using standard routines available in Analyze software (Brain Products). The data were band-pass filtered between 0.5 and 20 Hz. Manual sleep-stage scoring was performed for each 12-second interval by an experienced polysomnographic technologist (D.P.) using standard sleep-scoring criteria (57).

fMRI Data Preprocessing. Datasets were processed using custom routines written in IDL (ITT Visual Information Solutions) unless otherwise indicated. First, slice-timing correction was applied to the EPI data, and these images were registered to the first image of the short EPI run that included several TE values. Both corrections were performed using SPM2 software (Wellcome Department of Cognitive Neurology, London, United Kingdom). Distortion correction was performed using a field map computed from the 10 different TEs of the short EPI run (58). This correction was necessary because of the geometric distortions that were caused by using a low bandwidth to decrease acoustic noise. Remaining distortion was corrected by nonlinearly deforming the EPI data to match the undistorted FSE images using AIR 5.2.5 software (59). Physiological noise was corrected by modeling the cardiac rate, respiratory rate, and respiratory envelope and regressing out the activity associated with these variables (60, 61), together with a baseline regressor of third-order polynomial functions. A high-pass filter (0.005 Hz) was applied to remove any baseline drifts. The functional data were transformed to a standardized space using SPM8 (Wellcome Department of Cognitive Neurology, London, United Kingdom): for each subject, MPRAGE images were coregistered to FSE images. Then, MPRAGE images were spatially normalized to the Montreal Neurological Institute (MNI) space (62) using the unified segmentation algorithm implemented in SPM8. The normalization parameters generated in this step were subsequently applied to the EPI data. The EPI data were then resampled to $3 \times 3 \times 3$-mm^3 spatial resolution.

1. Vogt BA, Laureys S (2005) Posterior cingulate, precuneal and retrosplenial cortices: Cytology and components of the neural network correlates of consciousness. *Prog Brain Res* 150:205–217.
2. Vanhaudenhuyse A, et al. (2010) Default network connectivity reflects the level of consciousness in non-communicative brain-damaged patients. *Brain* 133(Pt 1): 161–171.
3. Koike T, Kan S, Misaki M, Miyauchi S (2011) Connectivity pattern changes in default-mode network with deep non-REM and REM sleep. *Neurosci Res* 69(4):322–330.
4. Horovitz SG, et al. (2009) Decoupling of the brain's default mode network during deep sleep. *Proc Natl Acad Sci USA* 106(27):11376–11381.
5. Sämann PG, et al. (2011) Development of the brain's default mode network from wakefulness to slow wave sleep. *Cereb Cortex* 21(9):2082–2093.
6. Spoormaker VI, et al. (2010) Development of a large-scale functional brain network during human non-rapid eye movement sleep. *J Neurosci* 30(34):11379–11387.
7. Larson-Prior LJ, et al. (2011) Modulation of the brain's functional network architecture in the transition from wake to sleep. *Prog Brain Res* 193:277–294.
8. Christoff K, Gordon AM, Smallwood J, Smith R, Schooler JW (2009) Experience sampling during fMRI reveals default network and executive system contributions to mind wandering. *Proc Natl Acad Sci USA* 106(21):8719–8724.
9. Mason MF, et al. (2007) Wandering minds: The default network and stimulus-independent thought. *Science* 315(5810):393–395.
10. Vincent JL, et al. (2007) Intrinsic functional architecture in the anaesthetized monkey brain. *Nature* 447(7140):83–86.
11. Kobayashi Y, Amaral DG (2003) Macaque monkey retrosplenial cortex: II. Cortical afferents. *J Comp Neurol* 466(1):48–79.
12. Kobayashi Y, Amaral DG (2007) Macaque monkey retrosplenial cortex: III. Cortical efferents. *J Comp Neurol* 502(5):810–833.
13. Petrides M, Pandya DN (2007) Efferent association pathways from the rostral prefrontal cortex in the macaque monkey. *J Neurosci* 27(43):11573–11586.
14. Buckwalter JA, Parvizi J, Morecraft RJ, van Hoesen GW (2008) Thalamic projections to the posteromedial cortex in the macaque. *J Comp Neurol* 507(5):1709–1733.
15. Baleydier C, Mauguiere F (1985) Anatomical evidence for medial pulvinar connections with the posterior cingulate cortex, the retrosplenial area, and the posterior parahippocampal gyrus in monkeys. *J Comp Neurol* 232(2):219–228.
16. Tekian A, Afifi AK (1981) Efferent connections of the pulvinar nucleus in the cat. *J Anat* 132(Pt 2):249–265.
17. Guillery RW (1995) Anatomical evidence concerning the role of the thalamus in corticocortical communication: A brief review. *J Anat* 187(Pt 3):583–592.
18. Grieve KL, Acuña C, Cudeiro J (2000) The primate pulvinar nuclei: Vision and action. *Trends Neurosci* 23(1):35–39.
19. Posner MI (2012) Imaging attention networks. *Neuroimage* 61(2):450–456.
20. Shallice T (2002) *Fractionation of the Supervisory System. Principles of Frontal Lobe Function*, eds Stuss DT, Knight RT (Oxford Press, Oxford), pp 261–277.
21. Braun AR, et al. (1997) Regional cerebral blood flow throughout the sleep-wake cycle. An H2(15)O PET study. *Brain* 120(Pt 7):1173–1197.
22. Hong CC, Gillin JC, Dow BM, Wu J, Buchsbaum MS (1995) Localized and lateralized cerebral glucose metabolism associated with eye movements during REM sleep and wakefulness: A positron emission tomography (PET) study. *Sleep* 18(7):570–580.
23. Nofzinger EA, Mintun MA, Wiseman M, Kupfer DJ, Moore RY (1997) Forebrain activation in REM sleep: An FDG PET study. *Brain Res* 770(1–2):192–201.

24. Maquet P, et al. (1996) Functional neuroanatomy of human rapid-eye-movement sleep and dreaming. *Nature* 383(6596):163–166.
25. Maquet P, et al. (2000) Experience-dependent changes in cerebral activation during human REM sleep. *Nat Neurosci* 3(8):831–836.
26. Wehrle R, et al. (2005) Rapid eye movement-related brain activation in human sleep: A functional magnetic resonance imaging study. *Neuroreport* 16(8):853–857.
27. Miyauchi S, Misaki M, Kan S, Fukunaga T, Koike T (2009) Human brain activity time-locked to rapid eye movements during REM sleep. *Exp Brain Res* 192(4):657–667.
28. Wehrle R, et al. (2007) Functional microstates within human REM sleep: First evidence from fMRI of a thalamocortical network specific for phasic REM periods. *Eur J Neurosci* 25(3):863–871.
29. Kubota Y, et al. (2011) Dorsolateral prefrontal cortical oxygenation during REM sleep in humans. *Brain Res* 1389:83–92.
30. Aladjalova NA (1957) Infra-slow rhythmic oscillations of the steady potential of the cerebral cortex. *Nature* 179(4567):957–959.
31. Hughes SW, Lorincz ML, Parri HR, Crunelli V (2011) Infraslow (<0.1 Hz) oscillations in thalamic relay nuclei basic mechanisms and significance to health and disease states. *Prog Brain Res* 193:145–162.
32. Vanhatalo S, et al. (2004) Infraslow oscillations modulate excitability and interictal epileptic activity in the human cortex during sleep. *Proc Natl Acad Sci USA* 101(14):5053–5057.
33. Biswal B, Yetkin FZ, Haughton VM, Hyde JS (1995) Functional connectivity in the motor cortex of resting human brain using echo-planar MRI. *Magn Reson Med* 34(4):537–541.
34. Raichle ME, et al. (2001) A default mode of brain function. *Proc Natl Acad Sci USA* 98(2):676–682.
35. Beckmann CF, DeLuca M, Devlin JT, Smith SM (2005) Investigations into resting-state connectivity using independent component analysis. *Philos Trans R Soc Lond B Biol Sci* 360(1457):1001–1013.
36. Greicius MD, Krasnow B, Reiss AL, Menon V (2003) Functional connectivity in the resting brain: A network analysis of the default mode hypothesis. *Proc Natl Acad Sci USA* 100(1):253–258.
37. He BJ, Raichle ME (2009) The fMRI signal, slow cortical potential and consciousness. *Trends Cogn Sci* 13(7):302–309.
38. Achermann P, Borbély AA (1997) Low-frequency (< 1 Hz) oscillations in the human sleep electroencephalogram. *Neuroscience* 81(1):213–222.
39. Nir Y, et al. (2011) Regional slow waves and spindles in human sleep. *Neuron* 70(1):153–169.
40. Picchioni D, et al. (2011) Infraslow EEG oscillations organize large-scale cortical-subcortical interactions during sleep: A combined EEG/fMRI study. *Brain Res* 1374:63–72.
41. Sirieix C, Jouanneau M, Gervasoni D, Luppi P-H, Leger L (2010) Role of the rostral ventrolateral medulla in the regulation of paradoxical (REM) sleep in the rat. *SFN Annual Meeting, San Diego* (San Diego Convention Center, San Diego, CA) 300.21/KKK29.
42. Thankachan S, Lu J (2010) Neuronal activity of the mesencephalic locomotor region (MLR) during sleep-wake cycle in freely behaving rats. *SFN Annual Meeting, San Diego* (San Diego Convention Center, San Diego, CA) 300.6/KKK14.
43. Pearl PL, et al. (2002) Sawtooth wave density analysis during REM sleep in normal volunteers. *Sleep Med* 3(3):255–258.
44. Douglass AB, Benson K, Hill EM, Zarcone VP, Jr. (1992) Markovian analysis of phasic measures of REM sleep in normal, depressed, and schizophrenic subjects. *Biol Psychiatry* 31(6):542–559.
45. Morrison AR, Pompeiano O (1970) Vestibular influences during sleep. VI. Vestibular control of autonomic functions during the rapid eye movements of desynchronized sleep. *Arch Ital Biol* 108(1):154–180.
46. Quattrochi JJ, Mamelak AN, Binder D, Williams J, Hobson JA (1993) Dose-related suppression of REM sleep and PGO waves by the serotonin-1 agonist eltoprazine. *Neuropsychopharmacology* 8(1):7–13.
47. Terzano MG, Parrino L (2000) Origin and significance of the cyclic alternating pattern (CAP). REVIEW ARTICLE. *Sleep Med Rev* 4(1):101–123.
48. Hahn TT, Sakmann B, Mehta MR (2006) Phase-locking of hippocampal interneurons' membrane potential to neocortical up-down states. *Nat Neurosci* 9(11):1359–1361.
49. Crunelli V, Hughes SW (2010) The slow (<1 Hz) rhythm of non-REM sleep: A dialogue between three cardinal oscillators. *Nat Neurosci* 13(1):9–17.
50. Rauchs G, Desgranges B, Foret J, Eustache F (2005) The relationships between memory systems and sleep stages. *J Sleep Res* 14(2):123–140.
51. Ji D, Wilson MA (2007) Coordinated memory replay in the visual cortex and hippocampus during sleep. *Nat Neurosci* 10(1):100–107.
52. Dang-Vu TT, et al. (2008) Spontaneous neural activity during human slow wave sleep. *Proc Natl Acad Sci USA* 105(39):15160–15165.
53. Stickgold R, Hobson JA, Fosse R, Fosse M (2001) Sleep, learning, and dreams: Off-line memory reprocessing. *Science* 294(5544):1052–1057.
54. Stickgold R, James L, Hobson JA (2000) Visual discrimination learning requires sleep after training. *Nat Neurosci* 3(12):1237–1238.
55. Tononi G, Cirelli C (2003) Sleep and synaptic homeostasis: A hypothesis. *Brain Res Bull* 62(2):143–150.
56. Vertes RP (2004) Memory consolidation in sleep; Dream or reality. *Neuron* 44(1):135–148.
57. Rechtschaffen A, Kales A (1968) *A Manual of Standardized Terminology, Techniques and Scoring System for Sleep Stages of Human Subjects* (US National Institute of Neurological Diseases and Blindness, Neurological Information Network, Bethesda, MD).
58. Jezzard P, Balaban RS (1995) Correction for geometric distortion in echo planar images from B0 field variations. *Magn Reson Med* 34(1):65–73.
59. Woods RP, Grafton ST, Holmes CJ, Cherry SR, Mazziotta JC (1998) Automated image registration: I. General methods and intrasubject, intramodality validation. *J Comput Assist Tomogr* 22(1):139–152.
60. Shmueli K, et al. (2007) Low-frequency fluctuations in the cardiac rate as a source of variance in the resting-state fMRI BOLD signal. *Neuroimage* 38(2):306–320.
61. Birn RM, Diamond JB, Smith MA, Bandettini PA (2006) Separating respiratory-variation-related fluctuations from neuronal-activity-related fluctuations in fMRI. *Neuroimage* 31(4):1536–1548.
62. Tzourio-Mazoyer N, et al. (2002) Automated anatomical labeling of activations in SPM using a macroscopic anatomical parcellation of the MNI MRI single-subject brain. *Neuroimage* 15(1):273–289.

Fig. S1. Differences in functional connectivity of the PCC seed region when REM is contrasted with wakefulness (WAKE). Regions showing significantly higher correlation during REM than WAKE are indicated in orange and regions showing significantly higher correlation during WAKE than REM are indicated in blue (*P* < 0.05, corrected). Magnitudes of *t* statistics from the random effects analyses are indicated in the color bar and rendered on a single subject T1 image. Axial slices are displayed at the *z* axis levels indicated (in millimeters).
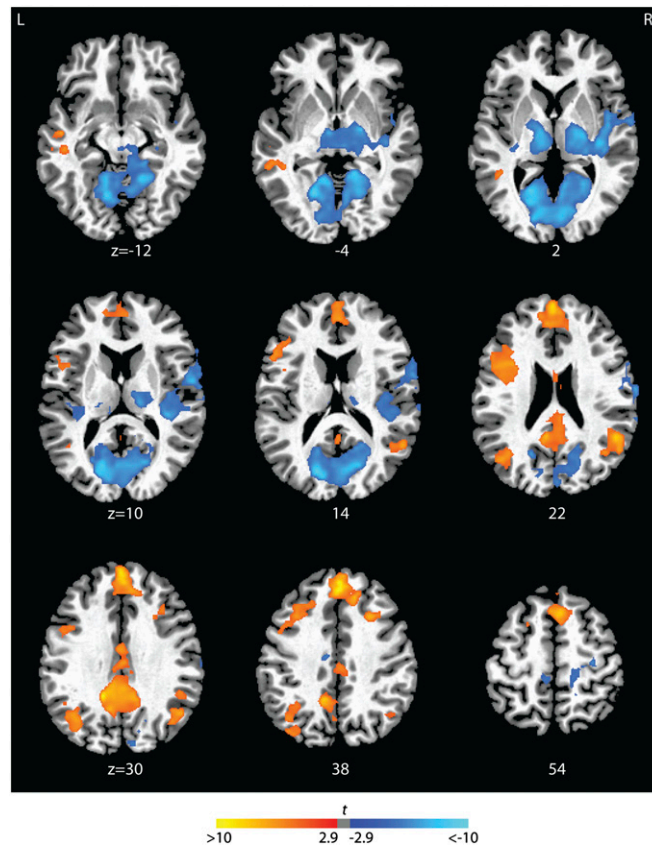
Fig. S2. Functional connectivity of the MPFC seed region during REM sleep. Brain regions correlated (orange) and anticorrelated (blue) with the MPFC seed during REM sleep (*P* < 0.05, corrected). Magnitudes of *t* statistics from the random effects analyses are indicated in the color bar and rendered on a single subject T1 image. Axial slices are displayed at the *z* axis levels indicated (in millimeter).
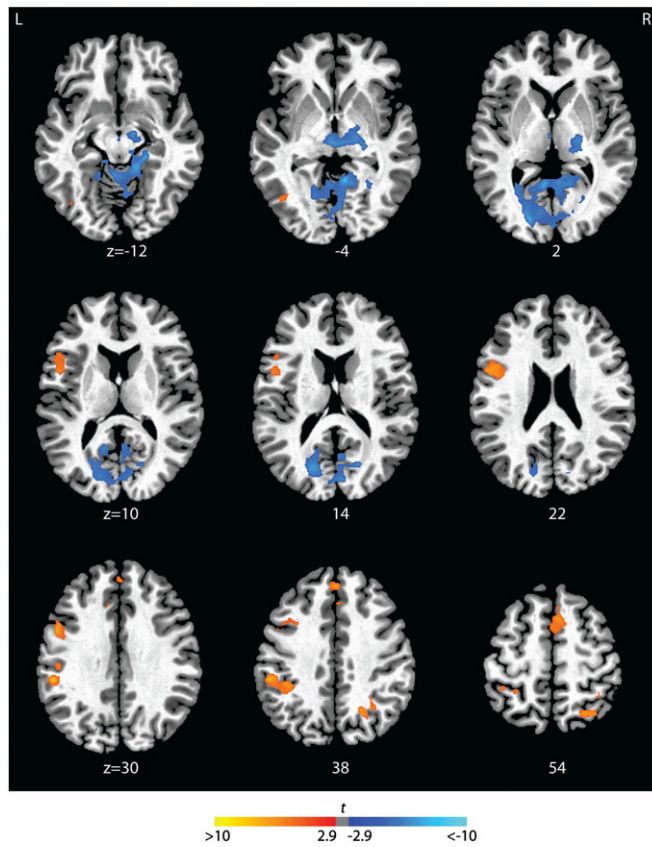
Fig. S3. Difference in functional connectivity of the MPFC seed region when REM is contrasted with WAKE. Regions showing significantly higher correlation during REM than WAKE are indicated in orange and regions showing significantly higher correlation during WAKE than REM are indicated in blue ($P < 0.05$, corrected). Magnitudes of t statistics from the random effects analyses are indicated in the color bar and rendered on a single subject T1 image. Axial slices are displayed at the z axis levels indicated (in millimeter).
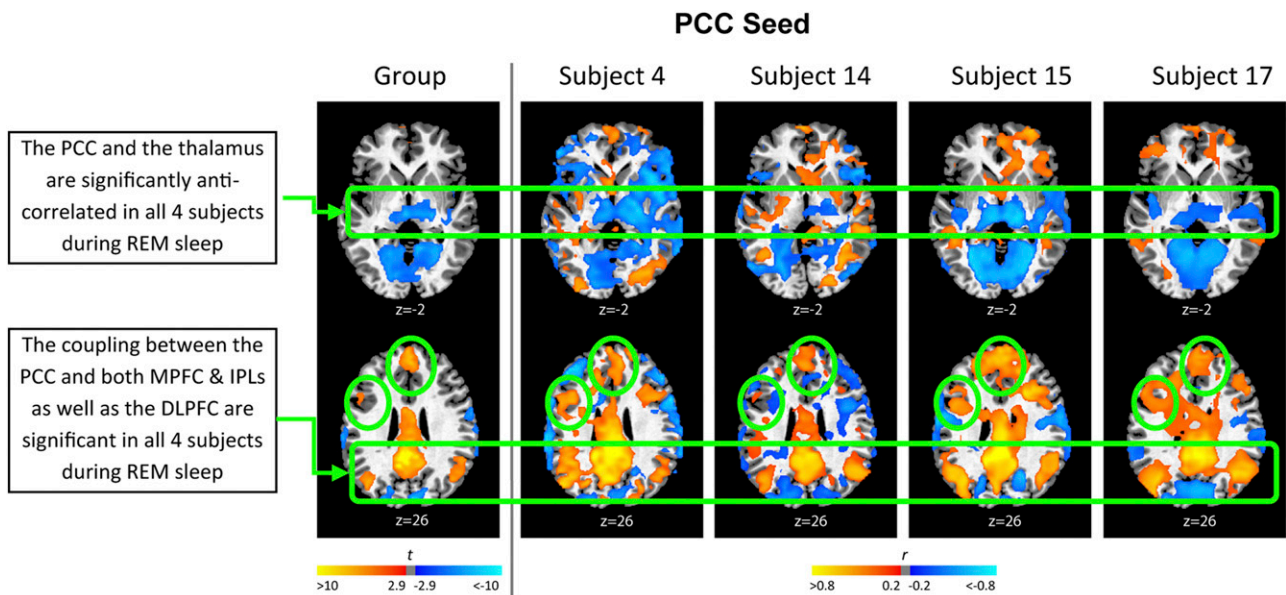

Fig. S4. Individual subject maps depicting correlations of the PCC seed region during REM sleep. Brain regions significantly correlated and anticorrelated with the PCC seed at corrected threshold $P < 0.05$ are indicated in orange and blue, respectively. Highly consistent across subjects, the PCC seed is significantly correlated with the elements within the DMN as well as additional heteromodal areas and anticorrelated with the thalamus and unimodal areas. Magnitudes of correlation are indicated in the color bar and rendered on a single subject T1 image. Axial slices are displayed at the z axis levels indicated (in millimeters).
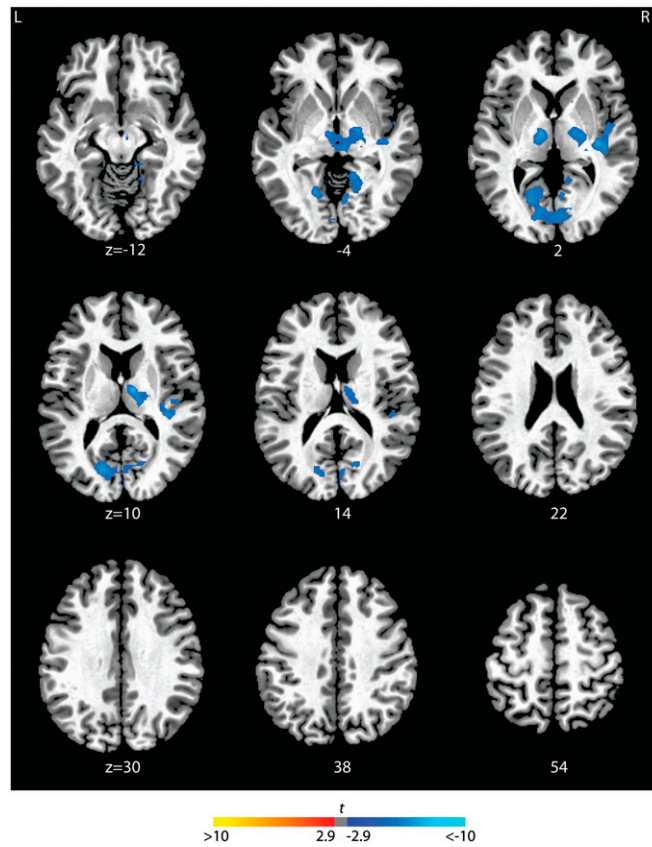
Fig. S5. Differences in functional connectivity of the thalamic seed region when REM is contrasted with WAKE. Regions showing significantly higher correlation during REM than WAKE are indicated in orange and regions showing significantly higher correlation during WAKE than REM are indicated in blue ($P < 0.05$, corrected). Magnitudes of t statistics from the random effects analyses are indicated in the color bar and rendered on a single subject T1 image. Axial slices are displayed at the z axis levels indicated (in millimeters). DLPFC, dorsolateral prefrontal cortex; IPL, inferior parietal lobule.
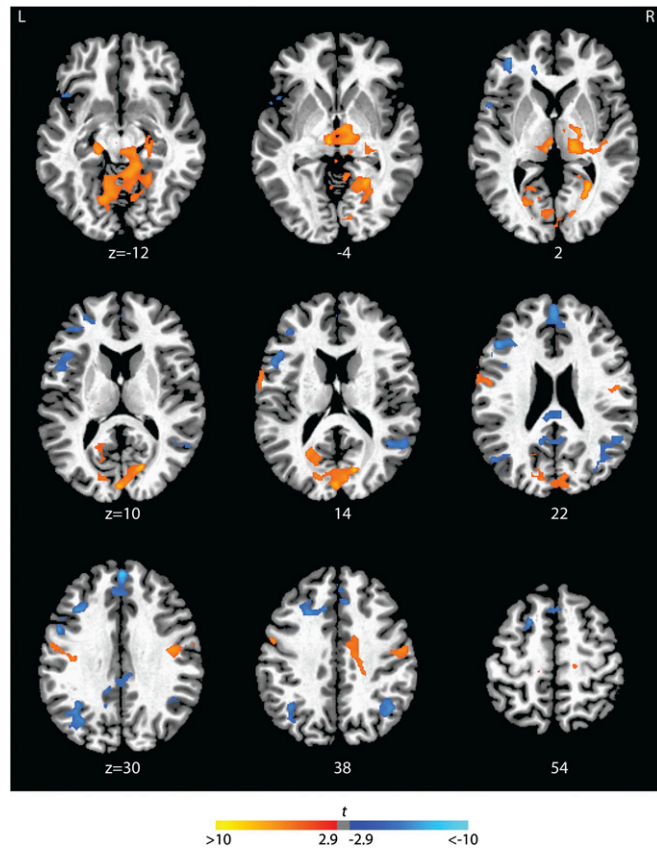
Table S1. Clusters of activity significantly correlated with the PCC seed during REM sleep, SWS, and WAKE

REM, SWS, and WAKE	L/R	mm³	x	y	z	t
REM						
Regions positively correlated with the PCC seed						
Cluster 1		36,450				
Precuneus	L		−6	−46	34	13.0
Posterior cingulate cortex	L		−3	−46	28	12.9
Cluster 2		30,942				
Medial prefrontal cortex (BA9)*,†	R		3	44	37	9.2
Medial prefrontal cortex (BA8)*,†	L/R		0	29	49	6.3
Dorsolateral prefrontal cortex/frontal eye fields*	L		−33	14	37	6.1
Dorsolateral prefrontal cortex	R		27	20	40	5.8
Inferior frontal gyrus*	L		−48	17	13	4.4
Cluster 3		6,993				
Inferior parietal lobule	R		48	−61	34	5.9
Cluster 4		4,887				
Inferior parietal lobule	L		−39	−70	25	6.7
Cluster 5		2,808				
Middle temporal gyrus	L		−54	−22	−8	6.7
Regions negatively correlated with the PCC seed						
Cluster 6		88,398				
Calcarine sulcus/cuneus*,†	R		9	−85	16	−10.6
Lingual gyrus*,†	R		15	−64	−8	−8.7
Lingual gyrus*,†	L		−17	−61	1	−6.5
Cerebellum*,†	L		−6	−64	−8	−9.3
Intralaminar thalamus*,†	R		6	−22	−5	−6.3
Thalamus (Pulvinar, VPL)*,†	R		18	−28	1	−6.3
Postcentral gyrus	R		63	−4	31	−6.7
Superior temporal gyrus (incl. Heschl gyrus)	R		66	−31	16	−6.5
SWS						
Regions positively correlated with the PCC seed						
Cluster 1		51,651				
Posterior cingulate cortex	L		−3	−46	28	21.6
Precuneus	R		−9	−55	28	17.7
Cluster 2		10,449				
Inferior parietal lobule	R		48	−61	37	8.6
Cluster 3		8,478				
Inferior parietal lobule	L		−36	−67	37	6.2
Regions negatively correlated with the PCC seed						
Cluster 4		1,107				
Insula	R		45	11	−8	−6.3
WAKE						
Regions positively correlated with the PCC seed						
Cluster 1		47,115				
Posterior cingulate cortex	L		−3	−49	25	16.6
Precuneus	L		−6	−46	34	15.0
Cluster 2		21,465				
Medial prefrontal cortex (BA10)	L/R		0	56	7	6.3
Superior frontal gyrus	R		18	38	40	6.1
Cluster 3		4,131				
Inferior parietal lobule	L		−42	−76	34	6.2
Cluster 4		3,348				
Inferior parietal lobule	R		45	−67	28	5.3
Regions negatively correlated with the PCC seed						
Cluster 5		22,059				
Postcentral sulcus	L		−54	−34	31	−10.6
Middle temporal gyrus	L		−57	−55	4	−9.4
Intraparietal sulcus	L		−33	−52	52	−6.7
Cluster 6		10,476				
Insula	L		−42	8	1	−7.7
Cluster 7		10,422				
Intraparietal sulcus	R		30	−52	46	−8.8
Cluster 8		10,206				
Inferior frontal gyrus	R		63	11	13	−8.0

Table S1. Cont.

REM, SWS, and WAKE	L/R	mm³	x	y	z	t
Dorsal premotor cortex	R		48	−4	49	−6.0
Insula	R		42	2	4	−5.9
Cluster 9		7,506				
Postcentral sulcus	R		60	−28	40	−10.7
Cluster 10		4,239				
Fusiform gyrus/lingual gyrus	L		−27	−58	−14	−5.6
Cluster 11		4,023				
Fusiform gyrus/lingual gyrus	R		15	−64	−8	−5.2
Cluster 12		2,943				
Frontal eye field	R		24	−7	52	−8.5
Cluster 13		1,944				
Superior occipital lobe	R		9	−88	25	−6.7

Anatomical location, hemisphere, cluster size, peak MNI coordinates and associated t statistics are tabulated.
*Significant difference observed between REM and WAKE within this region.
†Significant difference observed between REM and SWS within this region.

Table S2. Clusters of activity significantly correlated with the posterior thalamic seed during REM sleep, SWS, and WAKE

| REM, SWS, and WAKE	L/R	mm³	x	y	z	t
REM						
Regions positively correlated with the thalamic seed						
Cluster 1		32,382				
Thalamus*,†	L		−3	−22	1	19.1
Lingual gyrus*,†	R		27	−58	1	12.4
Lingual gyrus*,†	L		−16	−61	1	4.57
Cerebellum*,†	R		12	−40	−14	10.5
Calcarine sulcus/cuneus*,†	L		0	−88	10	8.2
Putamen	L		−24	−7	7	7.8
Putamen	R		24	5	4	5.9
Superior temporal gyrus (incl. Heschl gyrus)	R		42	−22	4	6.8
Posterior insula	L		−36	−31	16	4.7
Cluster 2		15,939				
Precentral gyrus*,†	R		21	−25	61	10.6
Precentral gyrus*	L		−51	−4	40	7.8
Middle cingulate cortex*	R		15	−13	40	7.2
Supplementary motor area	R		12	−10	70	6.0
Regions negatively correlated with the thalamic seed						
Cluster 3		11,169				
Dorsolateral prefrontal cortex*,†	L		−24	20	40	−9.9
Inferior frontal gyrus*,†	L		−54	11	13	−8.5
Anterior cingulate cortex*,†	L		−12	20	40	−5.8
Cluster 4		10,332				
Medial prefrontal cortex (BA9)*,†	R		3	53	28	−16.8
Medial prefrontal cortex (BA8) *,†	R		3	41	46	−11.2
Anterior insula	R		42	14	13	−10.2
Anterior middle frontal gyrus	R		33	59	7	−9.3
Dorsal premotor cortex	R		39	8	46	−7.53
Cluster 5		6,633				
Inferior parietal lobule*	R		42	−55	34	−8.5
Intraparietal sulcus	R		33	−64	52	−7.3
Fusiform/inferior temporal gyrus	R		39	−61	−8	−5.6
Cluster 6		5,787				
Inferior parietal lobule*	L		−39	−61	31	−9.3
Intraparietal sulcus	L		−33	−61	46	−5.6
Cluster 7		3,258				
Posterior cingulate cortex*	L		−12	−46	28	−7.6
Precuneus	L		−3	−70	49	−7.1
Cluster 8		2,628				
Fusiform/inferior temporal gyrus†	L		−42	−34	−20	−6.0
SWS						
Regions positively correlated with the thalamic seed						
Cluster 1		16,533				
Thalamus	L		−3	−22	1	21.7
Putamen	L		−24	−10	10	8.3
Putamen	R		27	−1	7	5.4
Cerebellum	R		9	−52	−17	8.8
Cluster 2		702				
Paracentral lobule	L		−3	−28	61	5.2
Cluster 3		180				
Middle cingulate cortex	R		12	−10	40	5.1
WAKE						
Regions positively correlated with the thalamic seed						
Cluster 1		7,137				
Thalamus	R		12	−19	1	9.5
Putamen	R		24	2	4	7.1
Putamen	L		−24	−7	7	5.5
Cluster 2						
Superior temporal gyrus (incl. Heschl gyrus)	R	1,494	57	−34	25	6.3
Cluster 3						
Insula	R	333	48	2	4	5.1

Anatomical location, hemisphere, cluster size, peak MNI coordinates and associated *t* statistics are tabulated.
*Significant difference observed between REM and WAKE within this region.
†Significant difference observed between REM and SWS within this region.

Table S3. Sleep parameters based on visual scoring in 12-second epochs

Subject	Total recording time (min)	Wake (min)	Stage 1 (min)	Stage 2 (min)	Stage 3 (min)	REM (min)	Total sleep time (min)
4	140.4	11.8	17.2	50.4	55.8	5.2	128.6
14	59.8	3.6	15.8	30.4	4.8	5.2	56.2
15	135.0	5.6	24.6	91.0	3.6	10.2	129.4
17	179.8	5.0	27.2	68.6	67.2	11.8	174.8
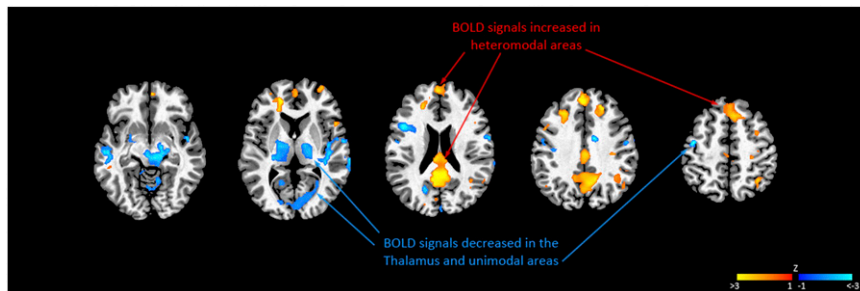
Movie S1. Video displaying temporal dynamics of hetermodal and unimodal regions during a continuous REM epoch (120 s) of a single subject. Standardized BOLD signals are masked by the group results are displayed on five selected axial slices (for details, see *Methods*). At each time point, increases in BOLD relative to the mean intensity of each voxel are indicated in orange and decreases are indicated in blue.

Movie S1